CONFIDENTIAL

NACA

RESEARCH MEMORANDUM

SUMMARY OF FREE-FLIGHT PERFORMANCE OF A SERIES OF RAM-JET

ENGINES AT MACH NUMBERS FROM 0.80 TO 2.20

By Warren J. North

Lewis Flight Propulsion Laboratory
Cleveland, Ohio

NATIONAL ADVISORY COMMITTEE
FOR AERONAUTICS
WASHINGTON
February 11, 1954

CONFIDENTIAL

2918

CW-1
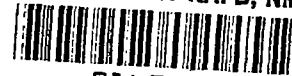
NATIONAL ADVISORY COMMITTEE FOR AERONAUTICS

RESEARCH MEMORANDUM

SUMMARY OF FREE-FLIGHT PERFORMANCE OF A SERIES OF RAM-JET

ENGINES AT MACH NUMBERS FROM 0.80 TO 2.20

By Warren J. North

SUMMARY

Data obtained from the NACA air-launched ram-jet program are summarized herein with emphasis placed upon the transonic propulsive thrust potential of the engines. Data are presented for boosted and nonboosted engine configurations which incorporate either a single-oblique-shock or a double-oblique-shock diffuser designed for critical inlet operation at flight Mach numbers of 1.8 and 2.4, respectively. The engines are evaluated in terms of flight Mach number, mass-flow ratio, diffuser pressure recovery, combustion-chamber heat release, propulsive thrust, external drag, and specific fuel consumption.

INTRODUCTION

During the past several years the NACA has investigated the performance capabilities of a series of free-flight ram-jet units which were air-launched from a carrier aircraft at high altitude. The fin-stabilized engine, which had no guidance equipment, followed a zero-lift trajectory. Performance data were obtained by means of telemetering and radar tracking.

Although it is usually considered that the supersonic ram jet would be rocket boosted to nearly the design Mach number, for such applications as air-launched missiles it may be advantageous for the ram jet to be self-accelerating from either a high subsonic or a low supersonic speed. The purpose of the investigations summarized herein has been to provide information on self-acceleration potentialities for fixed-geometry engines by obtaining data on full-scale supersonic engines at below design Mach numbers, particularly in the transonic range where theoretical calculations are questionable and ground test facilities for burning engines are nonexistent.

During these tests five basic fixed-geometry engines have been evaluated; four of the designs incorporated a single-oblique-shock inlet designed for Mach number 1.8, while the fifth utilized a double-oblique-shock inlet with a design point of 2.4. This latter model was boosted to approximately Mach number 1.5 prior to ram-jet ignition. In addition to the burning ram jets, several fully instrumented rocket-propelled cold models were flown for detailed drag evaluation at transonic Mach numbers. Specific performance results of the various models summarized herein are presented in references 1 to 8.

APPARATUS AND PROCEDURE

A B-29 airplane was used for launching the first two ram jets. All subsequent flights were conducted with an F-82 airplane (fig. 1).

In order to obtain maximum missile velocity at rocket burnout, it was desirable in the case of the drag models to launch at the highest possible altitude. From personnel considerations, 35,000 feet was set as maximum safe drop altitude for prolonged unpressurized flight. The launching altitude for the nonboosted ram-jet engines varied from 28,000 to 35,000 feet. The early models were mounted under the right wing of the F-82 airplane; however, the longer and heavier Mach number 2.4 model was moved to a center-wing mount, as this model mounted in the original missile location disturbed air flow over the outer-wing panel at high angles of attack, thereby providing marginal low-speed lateral control of the airplane.

The four models with single-oblique-shock inlet were designated 16-A, B, C, and D, and were designed for successively higher combustion-chamber-inlet Mach numbers ranging from 0.12 to 0.24 at total-temperature ratios τ of 4.0, 5.0, 3.9, and 3.0, all at a flight Mach number of 1.6. Models A and B used convergent exit nozzles, whereas C and D incorporated straight pipe exits. The double-oblique-shock inlet F models, which utilized a straight pipe exit, realized a critical τ of 3.0 with combustion-chamber-inlet Mach number of 0.24 at free-stream Mach number 2.0.

The oblique-shock inlet on the A, B, C, and D models incorporated a 50° cone; the cone was positioned to cause cowl-lip-shock intersection at a free-stream Mach number of 1.8. The diffuser annulus was designed with no internal contraction. The cowl lip external angle was 18°, which provides for shock attachment behind the cone shock at a free-stream Mach number of 1.8. The F model engine incorporated a double-oblique-shock inlet with cone half-angles of 22° and 35°. The cowl lip was positioned to intercept the oblique shocks at flight Mach number 2.4.

The ram-jet units consist of an outer shell with four aft-mounted stabilizing fins and a concentrically located body in the diffuser section which houses the telemetering equipment and the fuel system. Cutaway views of typical ram-jet units are shown in figures 2 and 3. FM-AM frequency-division telemetering was incorporated in the nose section. A typical eight-channel telemeter nose section is shown in figure 4.

A fuel nozzle manifold (fig. 5) and flame holder were located aft of the central island. Either the ducted-airfoil flame holder (fig. 6(a)) or the star type (fig. 6(b)) was used as indicated in table I. Magnesium flares provided a continuous ignition source. On the later models an electrically heated solid propellant booster rocket was mounted behind the flame holder; the rocket case is shown in figure 3. Table I includes booster duration and thrust information, that is, 6-3000 indicates 6 seconds burning time and 3000 pounds thrust. The spent booster was jettisoned from the burning models. In order to reduce combustion-chamber-inlet velocity during ram-jet ignition, a burn-out mass-flow restrictor was installed in the exit. The booster case remained in the nonburning drag models and the missile exit incorporated a faired annular restriction (fig. 7) in order to simulate mass flow associated with heat release in the combustion chamber.

A sketch of the F model fuel system is shown in figure 8. Fuel was contained in a cylindrical cast-aluminum tank which incorporated a free piston for fuel displacement. Fuel metering was accomplished by free-stream total-pressure regulation of high-pressure helium release. Models A, B, C, and D fuel expulsion was obtained from helium pressure which collapsed a flexible rubber fuel tank. The engines burned unleaded gasoline.

The A, B, C, and D nose section shells were formed from 1/10-inch mild steel. The F model nose section was spun from 1/8-inch 52S aluminum. Combustion-chamber shells and nozzles were 1/16-inch Inconel forward of the fins and 1/8-inch Inconel from the fin leading edge to the engine outlet. Model F utilized a 1/8-inch shell for the last $10\frac{1}{2}$ inches only. Aluminum fins of 1/4-inch thickness were cantilevered to the exhaust nozzle with riveted and spot-welded angles; the fin and attachment angles incorporated thermal expansion slots spaced at $1\frac{3}{16}$ inch intervals along the entire length of the nozzle-fin junction, as shown in figure 9. Engine gross weights varied from 525 to 800 pounds. Individual engine configuration details and external shell coordinates are listed in tables I and II.

In order to obtain starting and operational information to expedite flight development, an investigation at Mach number 1.4 was conducted

in the free-jet facility at the NACA Langley Pilotless Aircraft Research Station, Wallops Island, Virginia. The engine installation is shown in figure 9. The flame holder and combustion chamber were observed to be undamaged after several 40-second runs with combustion-chamber-exit total temperature near 3000° R. Forty seconds, which was the testing duration of the blow-down free-jet facility, was also the approximate duration of the missile flight.

Methods of calculation and a more complete description of apparatus and instrumentation are included in references 2, 7, and 8. Simulated T for the cold models was determined by calculating the heat release necessary to cause the same engine mass flow as was realized with the exit flow restrictors. Simulated thrust minus drag was then determined by subtracting observed external drag, exclusive of base drag, from a hypothetical internal thrust which was calculated from the previously determined value of simulated heat release. Additive drag was determined by the summation of axial force on the centerbody spike plus the gain in engine air flow axial momentum between the inlet and free stream.

SYMBOLS

The following symbols are used in this report:

A   maximum cross-sectional area, 1.4 sq ft

C_D drag coefficient, D/q_0A

C_F thrust coefficient, T/q_0A

D   drag, lb

f/a   fuel-air ratio

M   Mach number

m   mass flow

m_0 mass flow in free stream tube equal in area to projected lip area

P   total pressure, lb/sq ft absolute

p   static pressure, lb/sq ft absolute

q   dynamic pressure, lb/sq ft

T   thrust, lb

t   static temperature, $^{\circ}R$

V   velocity, ft/sec

W_f fuel flow, lb/hr

η_b combustion efficiency, percent

τ ratio of total temperature at the exhaust-nozzle outlet to total
     temperature at combustion-chamber inlet

Subscripts:

a   additive

c   cowl

f   friction

0   station at free stream

4   station at combustion-chamber inlet

RESULTS AND DISCUSSION

Diffuser Pressure Recovery

The supersonic single-shock conical inlet with a sharp-edged cowl
realized high values of subsonic and transonic total-pressure recovery
over a wide range of mass flows as shown in figure 10, which represents
the collective results obtained in flight from the A, B, C, and D
models. The indicated values of pressure recovery at zero mass-flow
ratio are those corresponding to normal shock, and dashed portions of
the curves indicate extrapolation of the data to these normal shock
values. Throughout the transonic region subcritical pressure recovery
decreases because of increasing friction losses as mass-flow ratio in-
creases. At the higher Mach numbers, the decreasing detached shock
losses overbalance the increasing friction losses, causing an increase
in subcritical pressure recovery as mass-flow ratio increases. As in-
dicated by the nearly vertical slopes of the curves in figure 10, total-
pressure recovery decreases rapidly as heat addition falls below the
critical value and the engine is subjected to high normal shock losses
inside the diverging diffuser. The maximum values of mass-flow ratio
shown for the various Mach numbers are the maximum values compatible
with free-stream flow deflection behind the conical shock or with inlet
choking. The maximum mass-flow ratio is equal to unity when the oblique

shock intersects the cowl at Mach number 1.8. The transonic data incorporated in figure 10 were obtained from both the burning and the cold models. At corresponding mass-flow ratios and Mach numbers, the pressure recovery obtained for the burning and nonburning engines agreed within 1 percent. The envelope curve, which encloses the knees of the pressure recovery curves, is indicative of the optimum mass-flow-ratio and Mach number combinations for which the normal shock stands at the diffuser inlet.

Figures 11 and 12 compare maximum pressure recoveries obtained in flight with those obtained in free-jet and wind tunnel tests of similar inlet configurations. These values of pressure recovery include subsonic diffuser friction loss. Good agreement between free-jet and flight performance for the single-cone diffuser is shown in figure 11. Pressure recovery values obtained in the 8- by 6-foot supersonic tunnel (ref. 9) fall slightly above the flight values. Although the tunnel tests were conducted at lower Reynolds numbers, the higher tunnel recoveries can be attributed to lower friction losses obtained with the shorter subsonic diffusers. A similar relation between flight and tunnel data, in the case of the double-oblique-shock inlet, is shown in figure 12. Comparison at Mach number 1.8 indicates that the double-oblique-shock diffuser yields a 5 percent greater recovery than the single-oblique-shock diffuser. Comparison of the theoretical recovery for the two engines indicates that, in part, the greater recovery of the two-cone diffuser is due to a more efficient subsonic diffuser. The increased subsonic efficiency in the two-cone inlet diffuser was probably due to a more rapid initial rate of expansion which minimized frictional losses due to high-velocity duct flow.

At Mach numbers above about 1.4, substantially subcritical operation was accompanied by diffuser pulsing, which in several cases appeared to cause engine blow-out. Transonic diffuser pulsing was noted with several models at near-critical operation. However, this instability can probably be attributed to combustor roughness due to low chamber pressures and overrich fuel-air ratios or to the unsatisfactory flame holder used initially (fig. 6(a)).

<div align="center">External Drag</div>

Detailed drag data from nonburning engines are presented in references 6 and 7. It was possible to correlate these cold-model drag data with those of the burning models by calculating simulated values of total-temperature ratios necessary to give the engine mass-flow ratios which were obtained by the use of cold-model mass-flow restrictors.

Figure 13(a) presents these data for the accelerating portion of one of the Mach number 1.8 drag model flights. The component external

2918

drags shown in figure 13(a) are those which would be realized by a burning ram jet with straight-pipe exit. The mass-flow-restrictor base pressure drag is not shown, since this drag component would not exist for the burning engine. As indicated by the negative values of cowl pressure drag coefficient, cowl suction occurs at Mach numbers less than 1.35 at the given mass-flow ratios. Cowl suction nearly offsets additive drag in the subsonic Mach number region. This result is to be expected since inviscid flow theory indicates that, subsonically, the sum of cowl suction and additive drag should equal zero.

The peak external drag coefficient occurred at Mach number 1.25 with the respective mass-flow ratio and simulated total-temperature ratio of 0.752 and 4.96. The friction drag is observed to constitute 73 percent of the drag at this point of maximum external drag coefficient. Since the maximum possible mass-flow ratio was 0.841 at Mach number 1.25, the diffuser was operating with 11 percent subcritical spillage.

Comparison of the burning (ref. 5) and nonburning drag data for a Mach number 1.8 model shows the burning model to have somewhat higher drag coefficient than the cold model under similar flow conditions. The discrepancy is attributed primarily to experimental error in determining the burning model drag coefficients, which were of necessity obtained by subtracting thrust-minus-drag from calculated internal thrust. Inasmuch as the thrust may be four times as great as the drag, a small error in the thrust or thrust-minus-drag calculation will result, percentagewise, in an appreciable error in drag coefficient.

Unpublished ram-jet drag data recently obtained with a Mach number 2.4 two-cone inlet are shown in figure 13(b) for model F-5. The peak external drag coefficient for this nonburning drag model reaches a value of 0.465 at a Mach number of 1.7. Additive drag is seen to comprise 73 percent of the peak external drag coefficient for the subcritical F engine, whereas friction accounts for only 24 percent. At this point of maximum external drag coefficient, the two-cone engine, designed for a τ of 3.0 but operating at a simulated τ of 4.5, spills 11 percent of the critical mass flow. Additive drag is somewhat offset by cowl suction in the transonic range, but due to the magnitude of additive drag, the sum of transonic additive and cowl pressure drags is greater than the corresponding drag coefficient measured on a Mach number 1.8 engine (fig. 13(a)).

Figure 14 indicates good correlation between component drag data as determined in free flight and in the 8- by 6-foot tunnel (ref. 9). Both models incorporated similar cowl configurations and 25° half-angle conical inlets designed for Mach number 1.8. For the range of mass-flow ratios investigated, the sum of cowl pressure drag and additive drag approaches zero as Mach number decreases toward unity. As would

be expected at constant supersonic Mach numbers, the sum of cowl pressure and additive drags increases as mass-flow ratio decreases.

Propulsive Thrust

The effect of free-stream Mach number and total-temperature ratio on A, B, C, and D model propulsive thrust coefficient is shown in figures 15(a) to (d), respectively. Positive values of propulsive thrust were obtained over a large range of total-temperature ratios for all values of free-stream Mach number encountered. During both subcritical and supercritical inlet operation, propulsive thrust increased as heat release increased.

If, for the purpose of this report, transonic is defined as the Mach number range from 0.9 to 1.3, the maximum observed transonic thrust-minus-drag coefficient for the burning models was 0.40. This value was attained by a D model with a total-temperature ratio of 5.1 and a Mach number of 0.92. The higher transonic values shown in figure 15(c) were simulated by a cold model. These values were obtained by the method described in APPARATUS AND PROCEDURE. A maximum over-all thrust-minus-drag coefficient of 0.53 was realized by a D model with a total-temperature ratio of 4.6 at Mach number 1.51.

The thrust-minus-drag coefficients obtained from the four single-cone models are compared at a common τ of 4.5 in figure 16. Transonic drag rise is responsible for the decrease in slope of the thrust-minus-drag coefficient curves as Mach number increases toward 1.0. The A and B curves show a pronounced dip at approximately Mach number 1.2. The dip indicates that in this Mach number range the added effect of base pressure drag on the convergent nozzle A and B models resulted in a transonic drag increase which exceeded the increase in thrust. The straight-pipe-exit C and D models attain approximately the same value of thrust minus drag at Mach numbers near design; however, the D model was somewhat superior in the transonic range. This transonic superiority was due mainly to higher diffuser pressure recovery at low mass-flow ratios. At any given Mach number in figure 16, the D engine realized a lower mass-flow ratio than the C engine by virture of its lower design τ. Since pressure loss associated with a detached shock becomes more severe at higher Mach numbers, the highly subcritical D engine thrust coefficient is penalized at near design Mach numbers; and the value of thrust minus drag approaches that of the C engine, which was operating somewhat subcritically at the common τ of 4.5.

It was possible to compare at $\tau = 3.0$ (fig. 17) the double-oblique-shock F engine with the D engine, which was the superior single-oblique-shock model from a propulsive thrust standpoint. At this τ both engines are operating with critical inlet flow at a free-stream Mach number

of 1.6. The F engine is seen to produce a propulsive thrust coefficient greater than that of the D engine at all Mach numbers greater than 1.7. In spite of a high value of additive drag below its design flight Mach number, the F engine realized the same propulsive thrust coefficient as the D engine at flight Mach number equal to 1.7, primarily because of the higher pressure recovery and corresponding high thrust coefficient associated with the double-oblique-shock diffuser.

In order to show the hypothetical acceleration potentialities of these engines, D and F model sea-level propulsive thrust is plotted as a function of Mach number in figure 18. The D curve was calculated from the coefficients shown on figure 16. The F curve corresponds to propulsive thrust coefficients at $\tau = 3.0$ (fig. 17). It can be seen that a 525-pound D model will accelerate vertically upward throughout the transonic Mach number range at low altitude.

In order to verify that thrust-minus-drag coefficient increases with an increase in τ during operation with subcritical inlet flow, the propulsive thrust coefficient of a burning model is compared in figure 19 with that of the drag model which used the greatest mass-flow restriction. The drag model (C-14) by virtue of higher simulated heat release realized simulated values of thrust-minus-drag coefficient higher than those obtained in the burning model. Both models were operating subcritically throughout the indicated Mach number range since the total-temperature ratios shown are higher than the design critical ratio of 3.9.

Propulsive Thrust Specific Fuel Consumption

Figure 20 shows the variation with Mach number of corrected propulsive thrust specific fuel consumption and the inverse relation, specific impulse, for the F model with approximately critical τ and for the C engine with slightly subcritical τ. The A, B, and D engines show similar trends. The data were obtained over a range of atmospheric temperatures from -75° to 100° F and have been corrected to -67° F, which is the standard temperature corresponding to the lower levels of the stratosphere.

The minimum value of propulsive thrust specific fuel consumption occurs at approximately design Mach number. As Mach number increases throughout the transonic range, the rapid decrease in specific fuel consumption is due to an increasing thrust-minus-drag coefficient and an increasing cycle efficiency as the compression ratio of the engine increases.

Although the F engine is subject to higher drag than the C model near Mach number 1.8, the propulsive specific fuel consumption is of

2918

CW-2

the same order because the double-oblique-shock F engine inlet realizes higher pressure recovery and because the F engine is designed to operate at a lower value of τ.

It is interesting to note that even at Mach number 1.0, the thrust-minus-drag specific impulse of the Mach 1.8 designed ram jets is approximately 500, or about 47 percent greater than the best theoretical rocket thrust specific impulse (ref. 12), indicating that for certain applications such as air-launched missiles with moderate range and pay load requirements the self-accelerating ram jet may have a lower gross weight than a ram jet with a rocket booster.

Combustor Performance

Due to the numerous variables involved - fuel pressure and temperature, fuel distribution, fuel nozzle type, flare-pilot heat release, fuel-air ratio, and combustor inlet conditions - no specific conclusions can be reached regarding effects of individual variables on combustor performance. As shown in figure 21, combustion efficiency was quite low at the minimum combustor pressures encountered; however, at a fuel-air ratio of 0.042, combustion efficiency increased from a value of 60 percent at a pressure of 3/4 atmosphere to 90 percent at a pressure of 4 atmospheres with corresponding combustor inlet temperatures of 540° to 850° R. Factors which probably contribute to the comparatively low combustion efficiencies at the lower pressures include poor fuel vaporization due to the low temperature of the fuel and low combustion inlet temperatures accompanying the low pressures.

With uniform type fuel distribution, a lean combustor limit of approximately 0.032 was observed for all pressures greater than about 1/2 atmosphere. Rich limits of about 0.058 to 0.08 were observed; the actual value varied appreciably with combustor inlet conditions.

During preflight tests in the Wallops Island Mach number 1.4 free-jet facility, maximum thrust was observed at a fuel-air ratio of 0.058. Additional increase in fuel-air ratio resulted in reduced thrust. Similar trends were observed in flight with about 0.055 to 0.06 fuel-air ratio appearing to be optimum.

SUMMARY OF RESULTS

Flight performance obtained from air-launched zero-lift trajectory ram jets, designed for optimum inlet operation at free-stream Mach numbers of 1.8 and 2.4, provided the following results:

1. The single-conical-shock-inlet fixed-geometry ram-jet engine demonstrated substantial positive values of transonic thrust minus drag and is therefore capable of self-acceleration throughout the transonic Mach number range.

2. From specific impulse considerations, it appears that for some air-launched missile applications the self-accelerating supersonic ram jet may have a lower gross weight than a rocket-boosted ram jet.

3. The supersonic conical inlet realized high values of subsonic and transonic total-pressure recovery throughout the range of subcritical and critical mass-flow ratios encountered. Under similar inlet flow conditions at Mach number 1.8, the double-oblique-shock diffuser total-pressure recovery was 5 percent higher than the single-shock-diffuser recovery.

4. Maximum external drag coefficient for a Mach number 1.8 nonburning engine occurred at Mach number 1.25, at which point friction drag constituted 73 percent of the external drag. Additive drag accounted for 73 percent of the peak external drag coefficient for a nonburning Mach number 2.4 engine.

5. The transonic propulsive thrust capabilities of the Mach number 1.8 engines are, in part, due to negative values of cowl pressure drag which offset additive drag during subcritical inlet operation.

6. The operable fuel-air-ratio limits ranged from 0.032 to approximately 0.08; the actual value of the rich limit varying appreciably with combustor inlet conditions.

7. Comparison of available free-flight, free-jet, and supersonic-tunnel data for similar ram-jet configurations indicates fairly good correlation of pressure recovery and external drag data.

Lewis Flight Propulsion Laboratory
    National Advisory Committee for Aeronautics
        Cleveland, Ohio, November 18, 1953

REFERENCES

1. Kinghorn, George F., and Disher, John H.: Free-Flight Investigation of 16-Inch-Diameter Supersonic Ram-Jet Unit. NACA RM E8A26, 1948.

2. Carlton, William W., and Messing, Wesley E.: Free-Flight Performance of 16-Inch-Diameter Supersonic Ram-Jet Units. I - Four Units Designed for Combustion-Chamber-Inlet Mach Number of 0.12 at Free-Stream Mach Number of 1.6 (Units A-2, A-3, A-4, and A-5). NACA RM E9F22, 1949.

3. Messing, Wesley E., and Simpkinson, Scott H.: Free-Flight Performance of 16-Inch-Diameter Supersonic Ram-Jet Units. II - Five Units Designed for Combustion-Chamber-Inlet Mach Number of 0.16 at Free-Stream Mach Number of 1.60 (Units B-1, B-2, B-3, B-4, and B-5). NACA RM E50B14, 1950.

4. Disher, John H., and Rabinowitz, Leonard: Free-Flight Performance of 16-Inch-Diameter Supersonic Ram-Jet Units. III - Four Units Designed for Combustion-Chamber-Inlet Mach Number of 0.245 at Free-Stream Mach Number of 1.8 (Units D-1, D-2, D-3, and D-4). NACA RM E50D07, 1950.

5. Rabb, Leonard, and North, Warren J.: Free-Flight Performance of 16-Inch-Diameter Supersonic Ram-Jet Units. IV - Performance of Ram-Jet Units Designed for Combustion-Chamber-Inlet Mach Number of 0.21 at Free-Stream Mach Number of 1.6 over a Range of Flight Conditions. NACA RM E50L18, 1951.

6. Messing, Wesley E., and Acker, Loren W.: Transonic Free-Flight Drag Results of Full-Scale Models of 16-Inch-Diameter Ram-Jet Engines. NACA RM E52B19, 1952.

7. Messing, Wesley E., and Rabb, Leonard: Transonic Free-Flight Investigation of the Total Drag and of the Component Drags (Cowl Pressure, Additive, Base, Friction, and Internal) Encountered by a 16-Inch-Diameter Ram-Jet Engine for Mach Numbers from 0.80 to 1.43. NACA RM E52F02, 1952.

8. Disher, John H., Kohl, Robert C., and Jones, Merle L.: Free-Flight Performance of a Rocket-Boosted, Air-Launched 16-Inch-Daimeter Ram-Jet Engine at Mach numbers up to 2.20. NACA RM E52L02, 1953.

9. Nussdorfer, T., Wilcox, F., and Perchonok, E.: Investigation at Zero Angle of Attack of a 16-Inch Ram-Jet Engine in the 8- by 6-Foot Supersonic Wind Tunnel. NACA RM E50L04, 1951.

10. Moeckel, W. E., Connors, J. F., and Schroeder, A. H.: Investigation of Shock Diffusers at Mach Number 1.85. II - Projecting Double-Shock Cones. NACA RM E6L13, 1947.

11. Triem, John S., and Rounds, Geo. L.: Interim Summary Report XRJ-43-MA-1 Supersonic Ramjet Research and Development Program. Rep. 5000, Marquardt Aircraft Co., Feb. 1948-Mar. 1950. (Proj. MX-702A, Air Force Contract W33-038ac-19050.)

12. Sutton, George P.: Rocket Propulsion Elements. John Wiley & Sons, Inc. (New York), 1949, p. 46.

2918

TABLE I. - RAM-JET CONFIGURATIONS

Models	Inlet area, sq ft	Exit area, sq ft	Boost	Burning or simulated	Flame holder	Design total-temperature ratio, τ	Combustion chamber design Mach number, M_4
A-1 to 5	0.270	0.68	None	Burning	A-1 to 4 ducted A-5 star	4.00	0.120
B-1 to 5	0.356	1.09	None	Burning	B-1 to 3 ducted B-4 and 5 star	5.00	0.160
C-1 to 5 and C-8	0.448	1.39	None	Burning	C-1 ducted C-2,5,8 star	3.90	0.210
C-13	0.448	1.39	14-1000	Burning	Star	4.00	0.210
C-10,11,14,16	0.448	0.419 to 0.573	14-1000	Simulated	None	4.00	0.210
D-1 to 4	0.553	1.39	None	Burning	Star	3.00	0.245
F-2	0.490	1.39	6-3000	Burning	Star	3.00	0.240
F-5	0.490	0.52	6-3000	Simulated	None	3.00	0.240

A-D models

F model
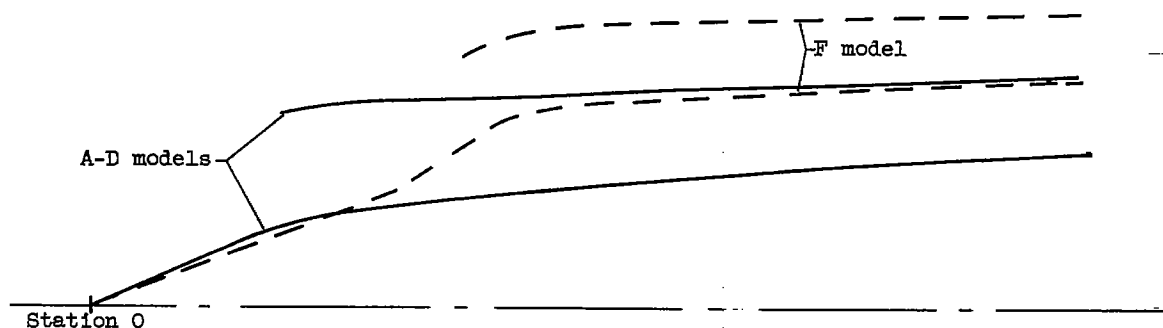
Station 0

TABLE II. - RAM-JET COORDINATES

Missile station, in.	Island outside radius		Shell outside radius				
	A-D, in.	F, in.	A, in.	B, in.	C, in.	D, in.	F, in.
0	0	0					
3.77	1.76	44° cone	4.00				
4.30	1.98	to sta-	4.17	4.56			
4.82	2.18	tion 7.88	4.32	4.72	5.13		
5.36	2.34	70° cone	4.42	4.85	5.27	5.56	
6.07	2.48	station	4.50	4.94	5.43	5.72	
6.55	2.57	7.88 to	4.55	4.99	5.47	5.81	
6.77	2.61	10.36	4.57	Conical	Conical	5.83	
7.11	2.64		Conical			5.85	
9.49	2.88					Conical	6.65
10.00	2.93						6.91
11.00	3.02	5.14					7.21
12.00	3.12	5.38					7.32
20.00	3.81	5.88					7.73
30.00	4.43	6.05					7.98
40.00	4.98	5.98					8.06
48.00	5.35	5.80	7.48				
51.00	5.45	5.75	7.58	7.68			
53.65	5.51	5.69	7.70	7.76	7.84		
58.77	5.47	5.56	7.96	7.98	7.99	8.04	
60.55	5.42	5.49	8.06	8.06	8.06	8.06	
70.00	4.72	5.12					
80.00	3.47	4.66					
90.00	1.64	4.01					
97.75	0	3.26					
110.00		0					
133.80							
136.55				8.02			
142.50			7.68	7.85			
168.00			6.59	7.19			
189.80							

2918

Figure 1. - Ram-jet engine mounted under F-82 center wing section. Loading vehicle in place.
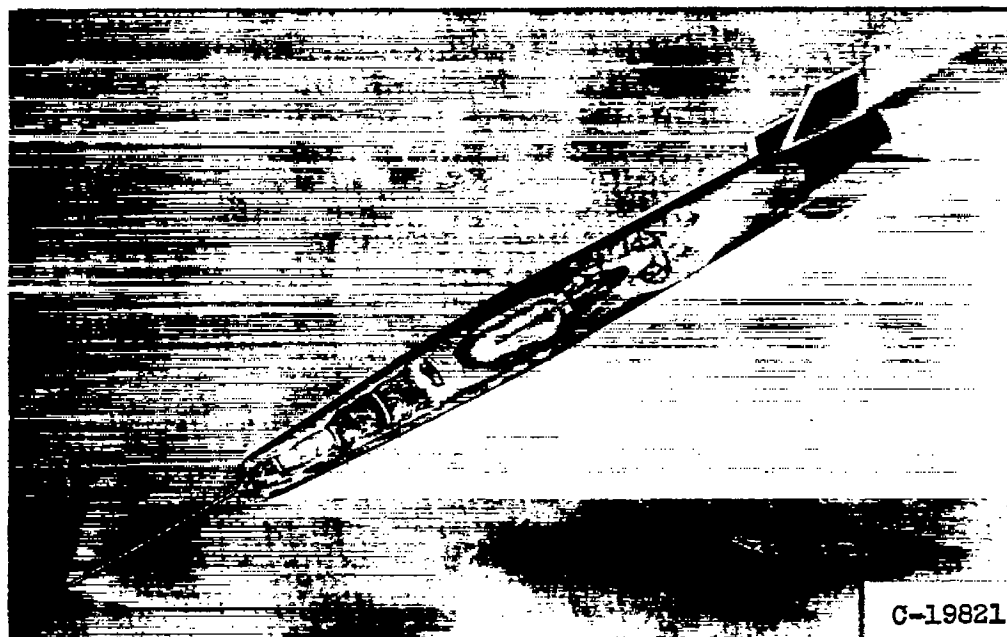
Figure 2. - Sketch of nonboosted B model in flight.

Station	Distance from pitot-static tip, in.
1	31.63
2	34.25
3	58.38
4	122.50
5	145.81
7	212.06

Instrument	Measurement
1	Axial net acceleration, positive (not shown)
2	Axial net acceleration, negative (not shown)
3	Fuel flow, low range
4	Fuel flow, high range
5	Free-stream total pressure (behind normal shock)
6	Free-stream static pressure

Instrument	Measurement
7	Static pressure in diffuser
8	Dynamic pressure in diffuser
9	Static pressure in diffuser
10	Total pressure in diffuser outlet
11	Total pressure at engine outlet
12	Static pressure at engine outlet

Figure 3. - Sketch of model F ram-jet engine showing major components, dimensions, and instrumentation. (All dimensions are in inches.)
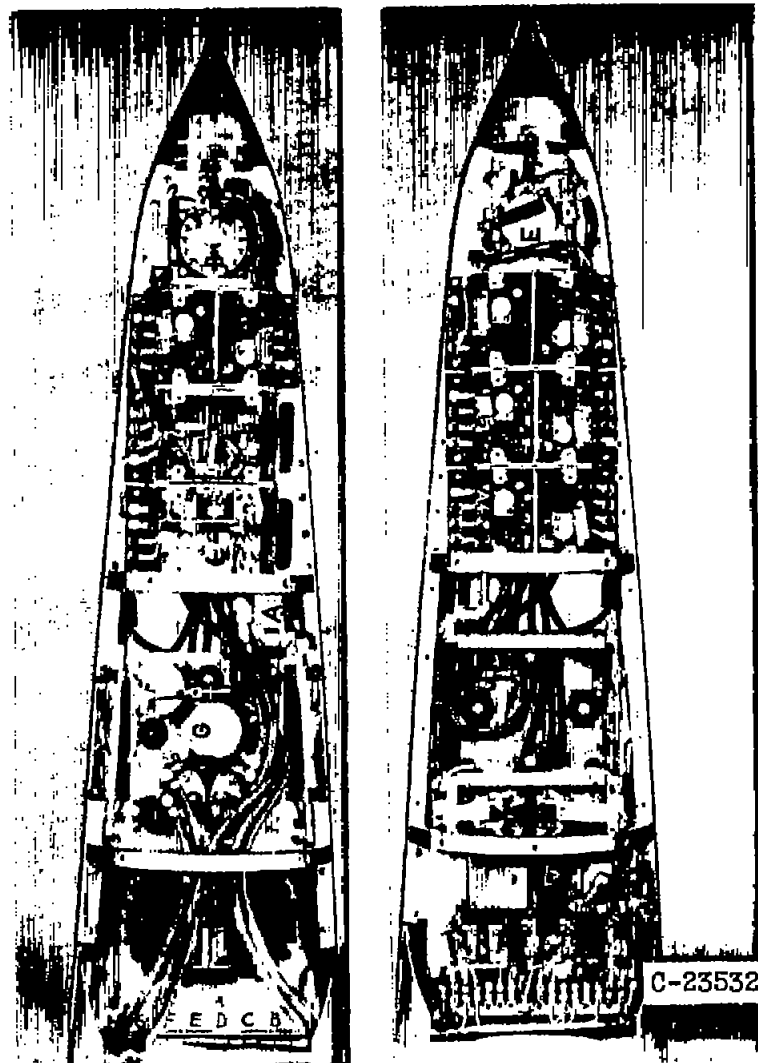
Figure 4. - Typical eight-channel telemeter nose section.
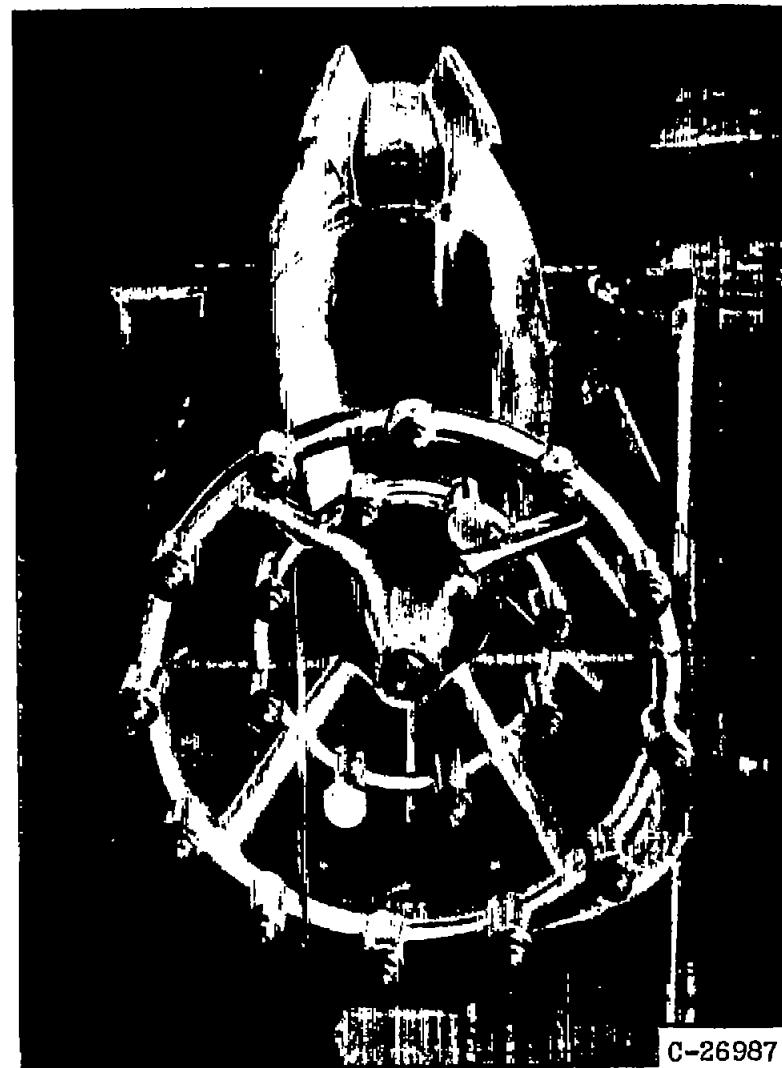
Figure 5. - Typical fuel-nozzle manifold.

(a) Ducted airfoil.
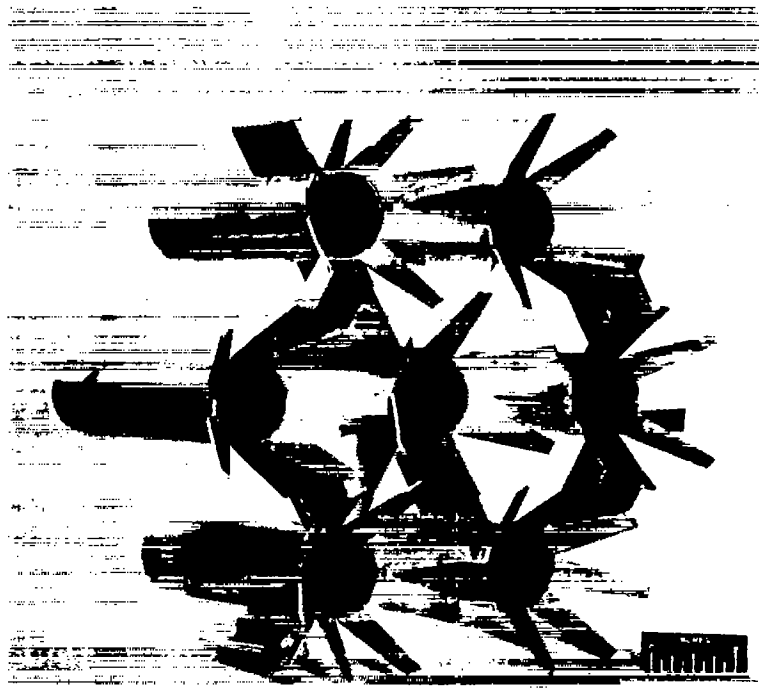
(b) Star-type.

Figure 6. - Flame holders.

CONFIDENTIAL
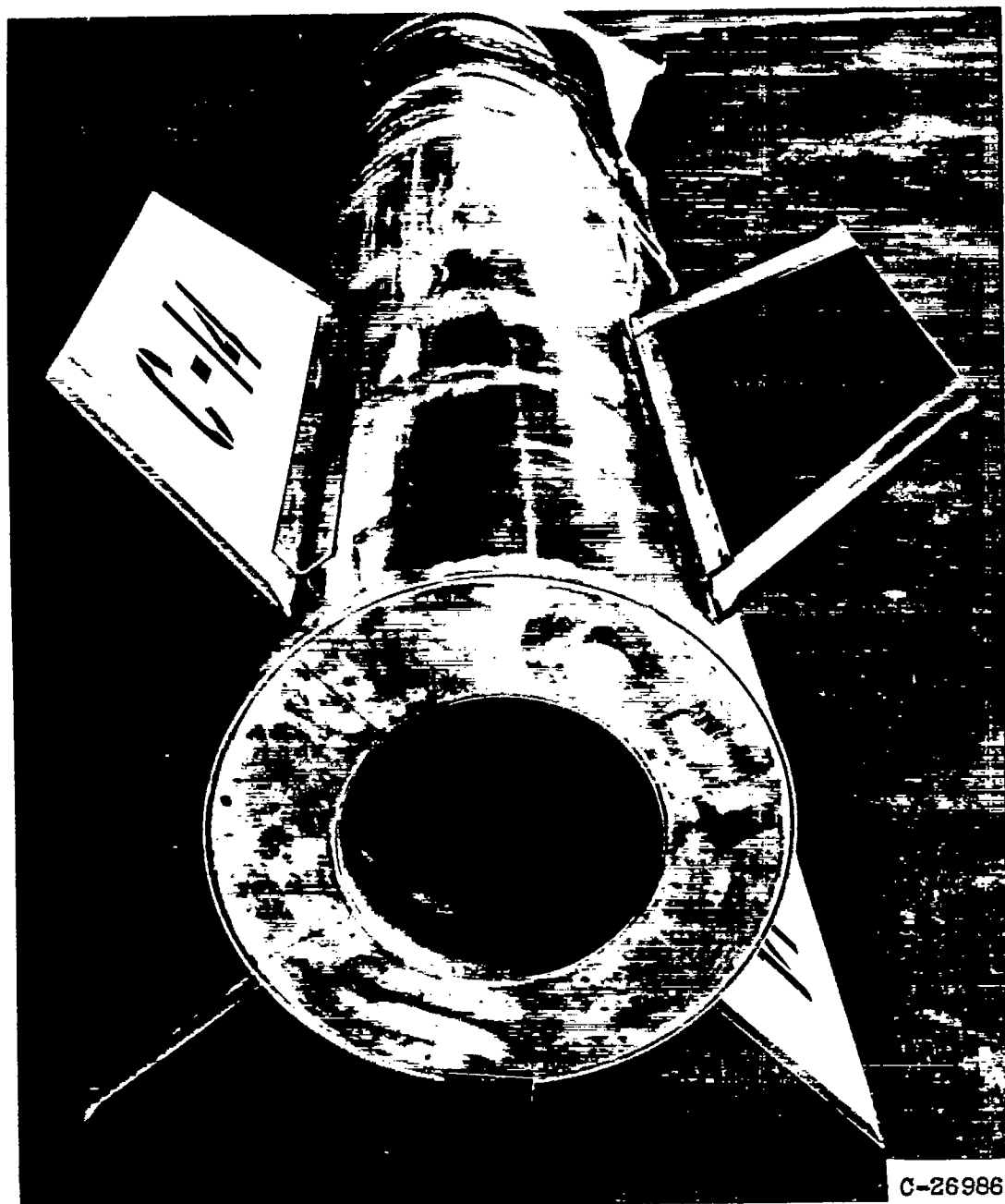
C-26986

Figure 7. - Exit flow restrictor incorporated on nonburning boosted drag models.

Bleed-off
port

First stage pressure
reduction (3500 to 800 psig)

High-pressure
inlet port

High-pressure helium
shut-off valve

Main fuel pressure
regulator

High pressure helium
storage (3500 psig)

Combustion chamber
static pressure

Free piston

Free-stream
total pressure

Regulated
helium supply

Fuel storage

Venturi

Pressure differential
measuring taps

Spring-loaded fuel
shut-off valve

Fuel manifold and
spray nozzles

CD-2802

Figure 8. - Fuel system used in model F ram-jet engine.
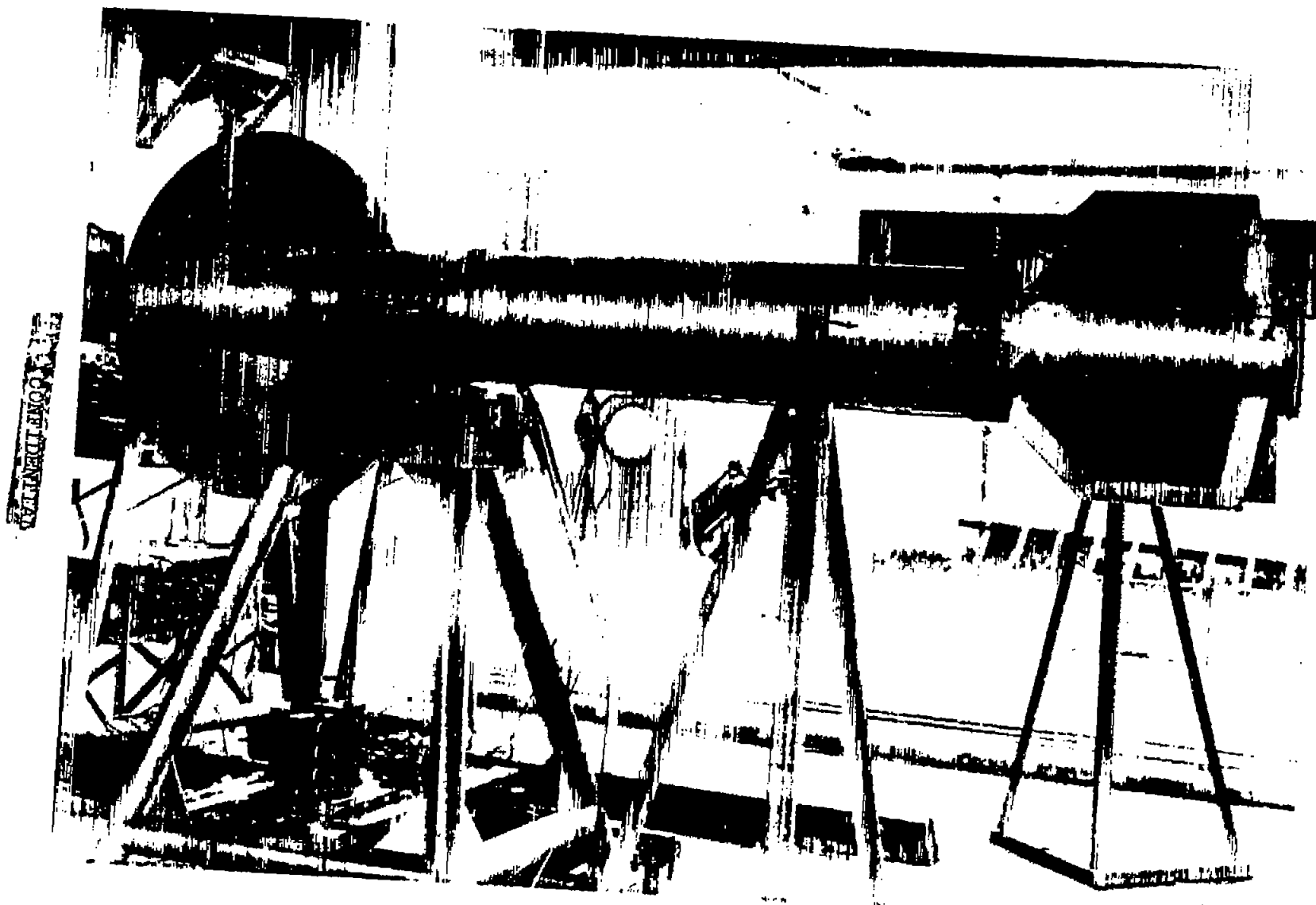
Figure 9. - Ram-jet engine installation at Wallops Island free-jet facility.

C-34262
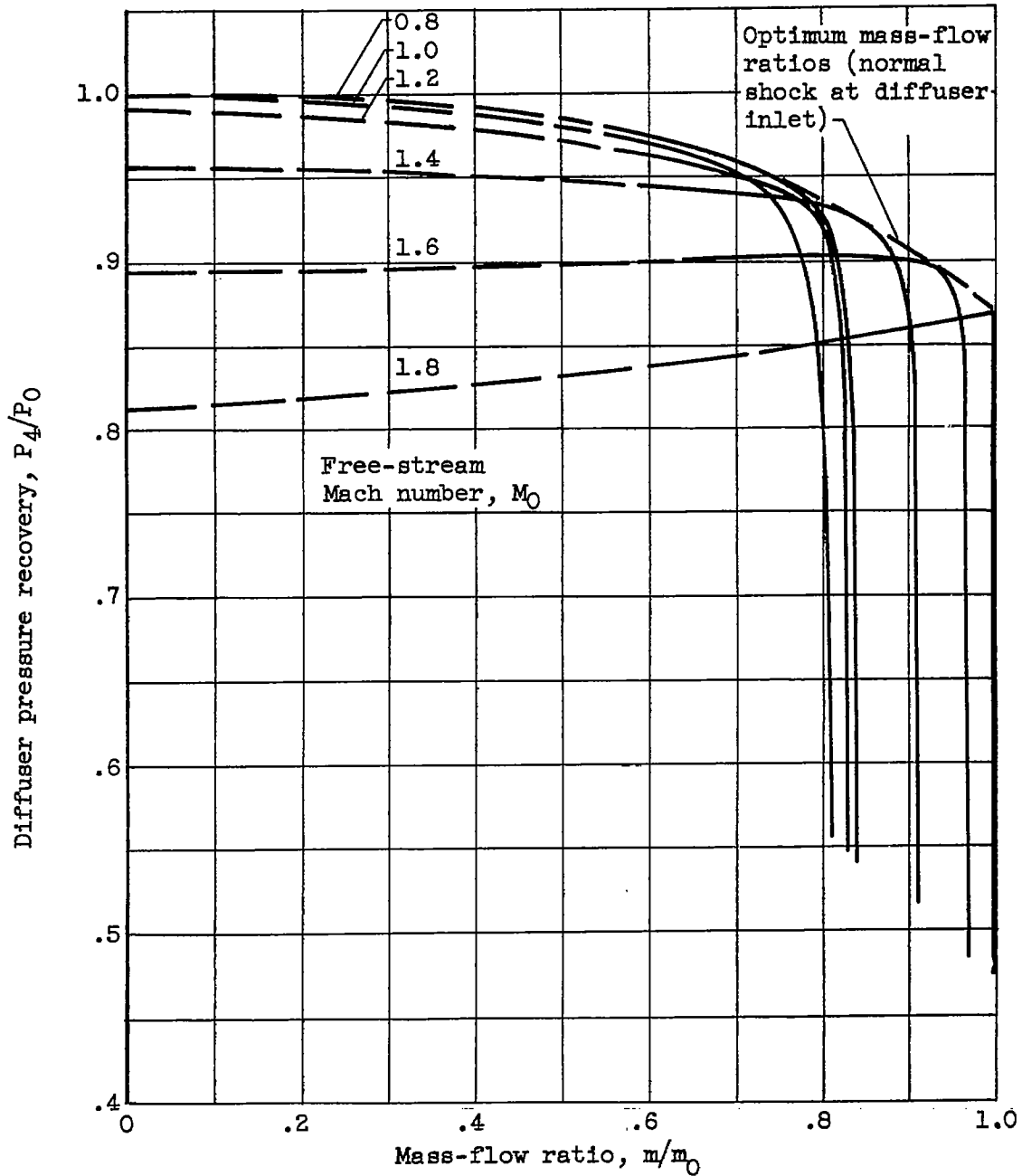
Figure 10. - Diffuser total-pressure recovery obtained with
A, B, C, and D models at various free-stream Mach numbers.
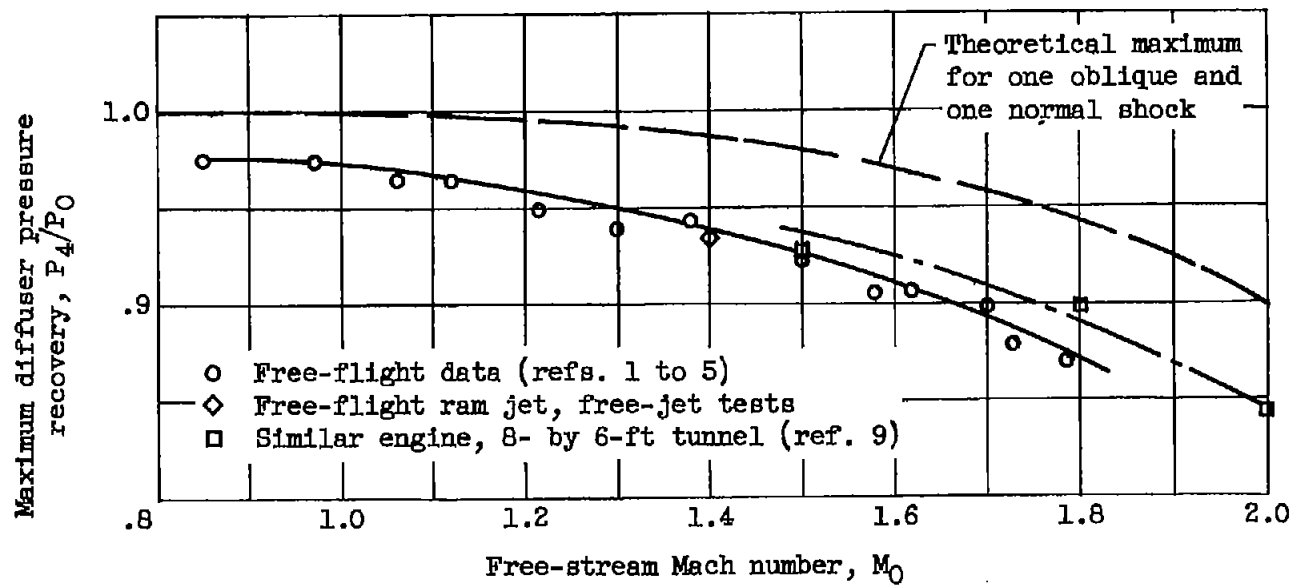
Figure 11. - Comparison of maximum diffuser pressure recovery for single-oblique-shock, 50° conical inlets.
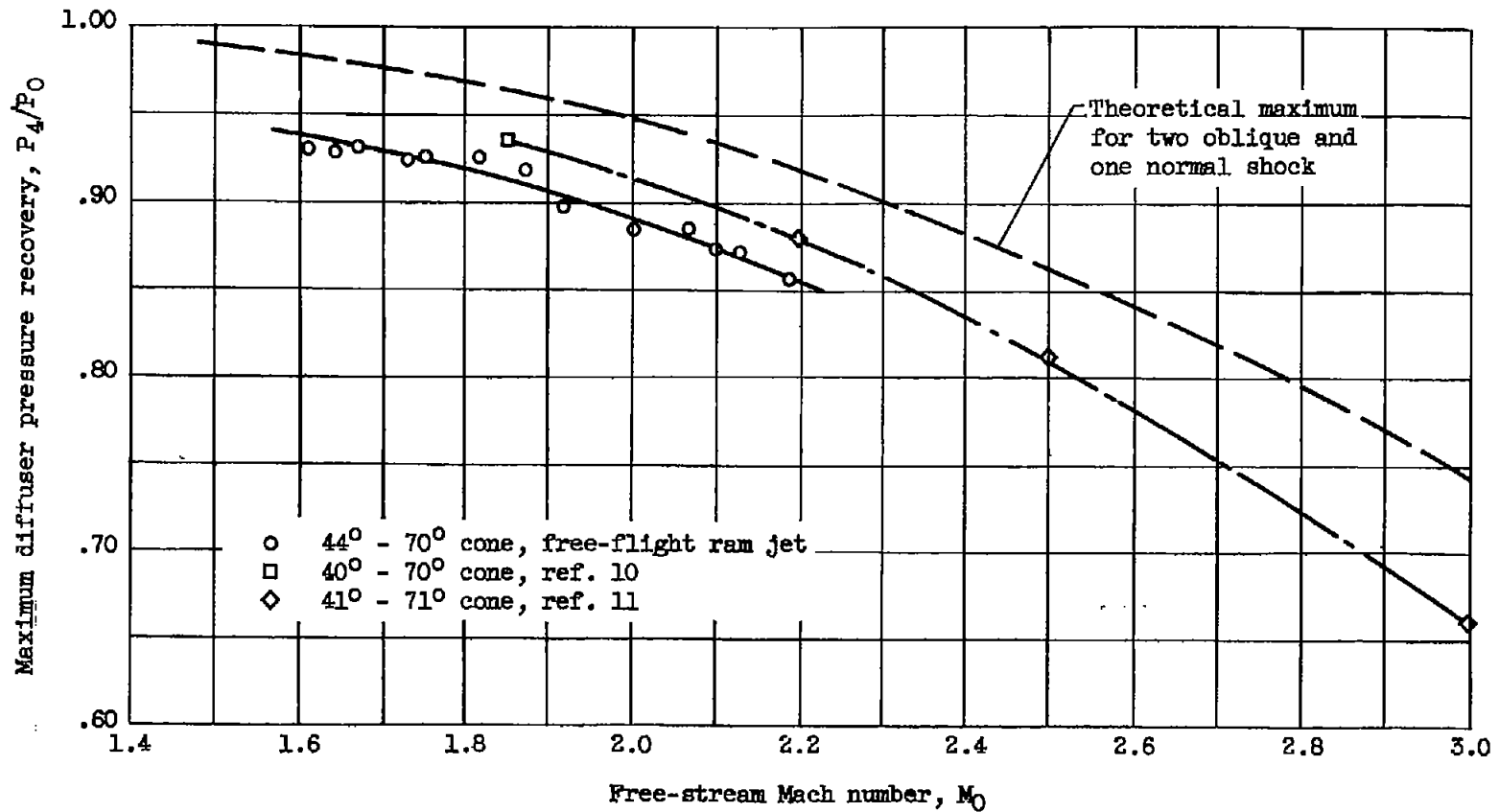
Figure 12. - Comparison of maximum diffuser pressure recovery for double-oblique-shock conical inlets.

2918

CW-4
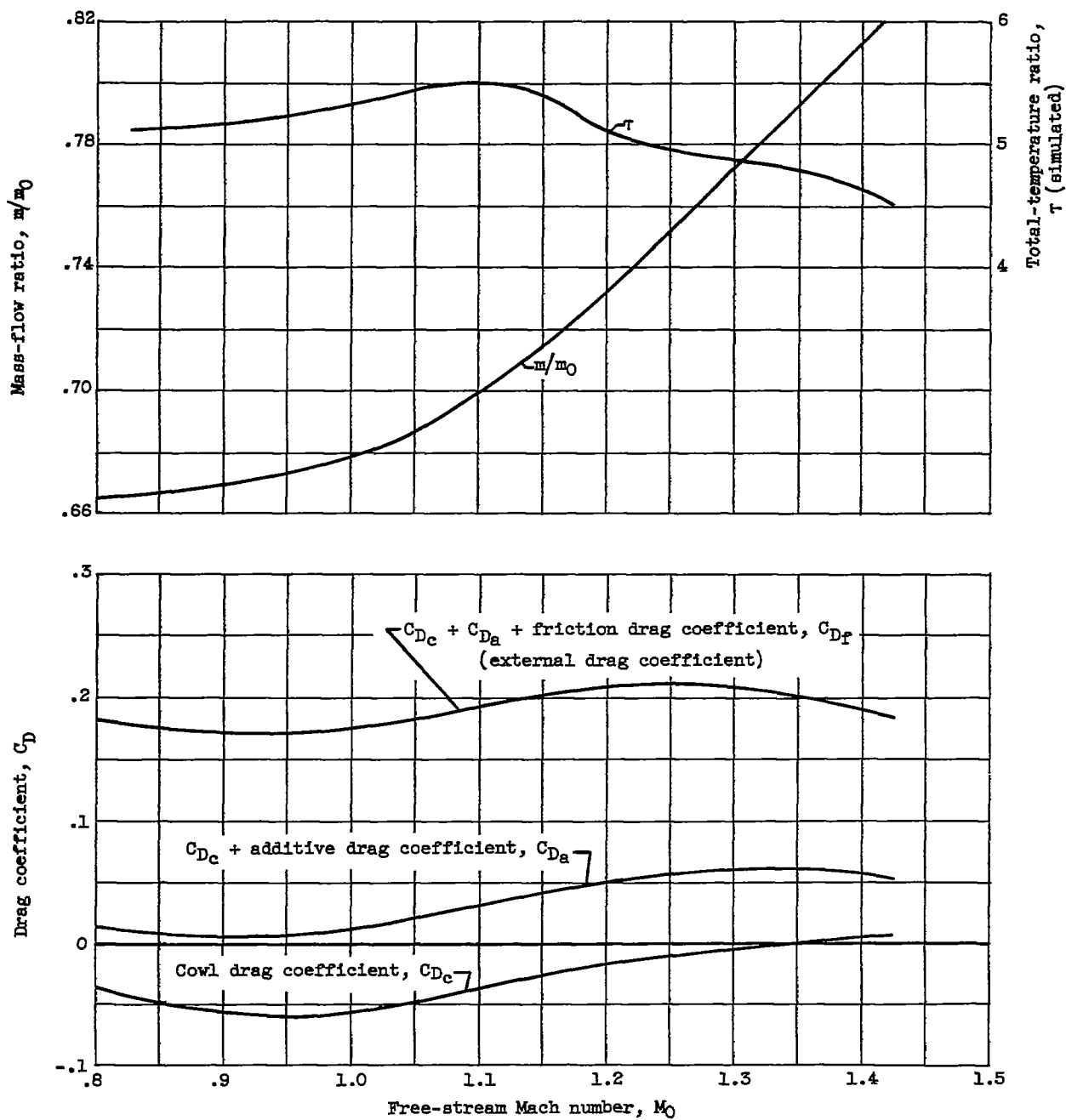
(a) Model C-16.

Figure 13. - Effect of Mach number and simulated total-temperature ratio on mass-flow ratio and component drag coefficients.
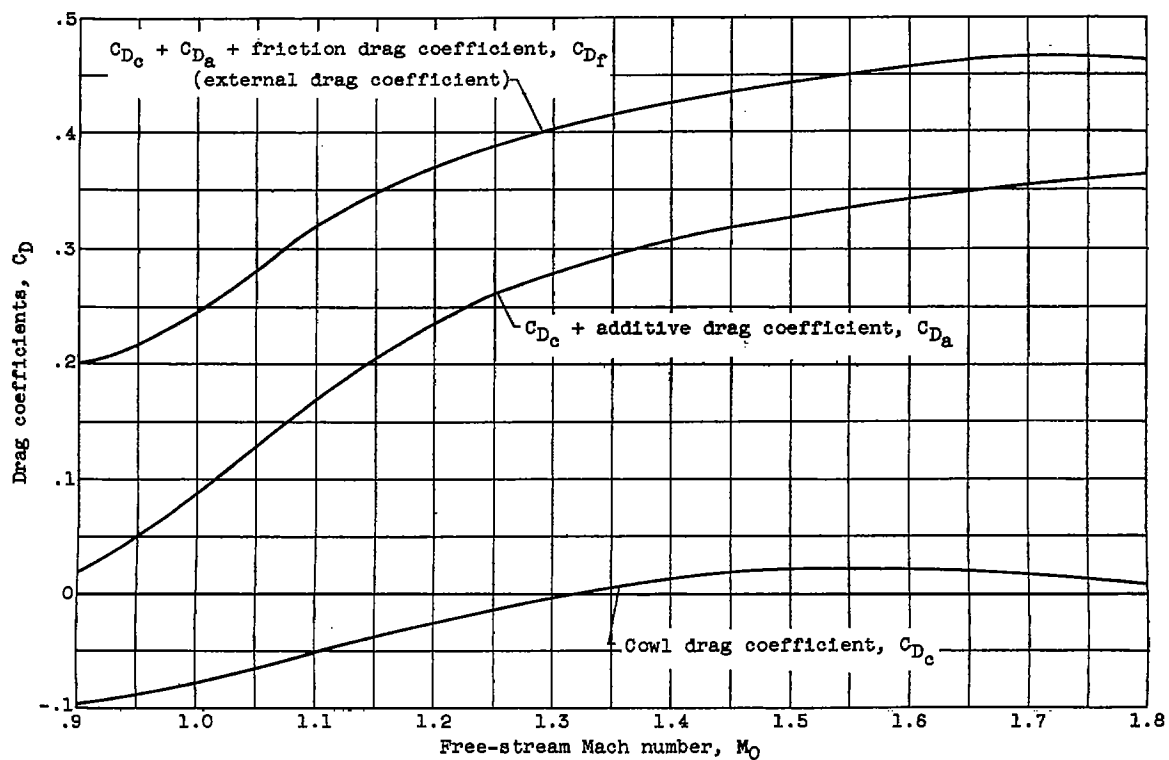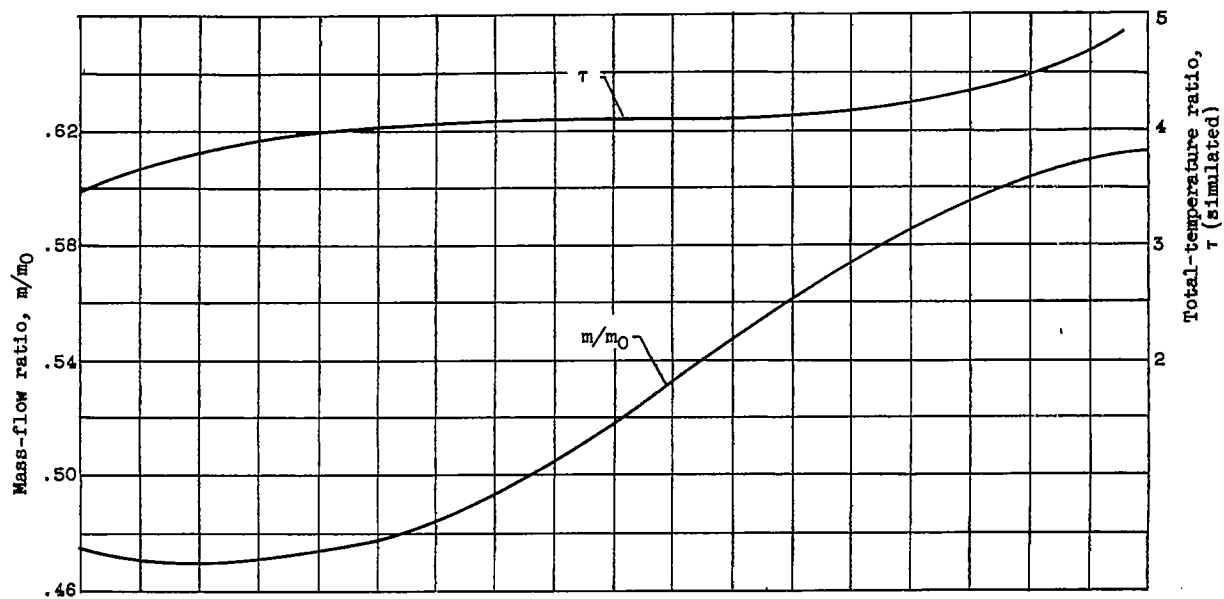
(b) Model F-5.

Figure 13. - Concluded. Effect of Mach number and simulated total-temperature ratio on mass-flow ratio and component drag coefficients.

29''

ĊW-4 bȧck
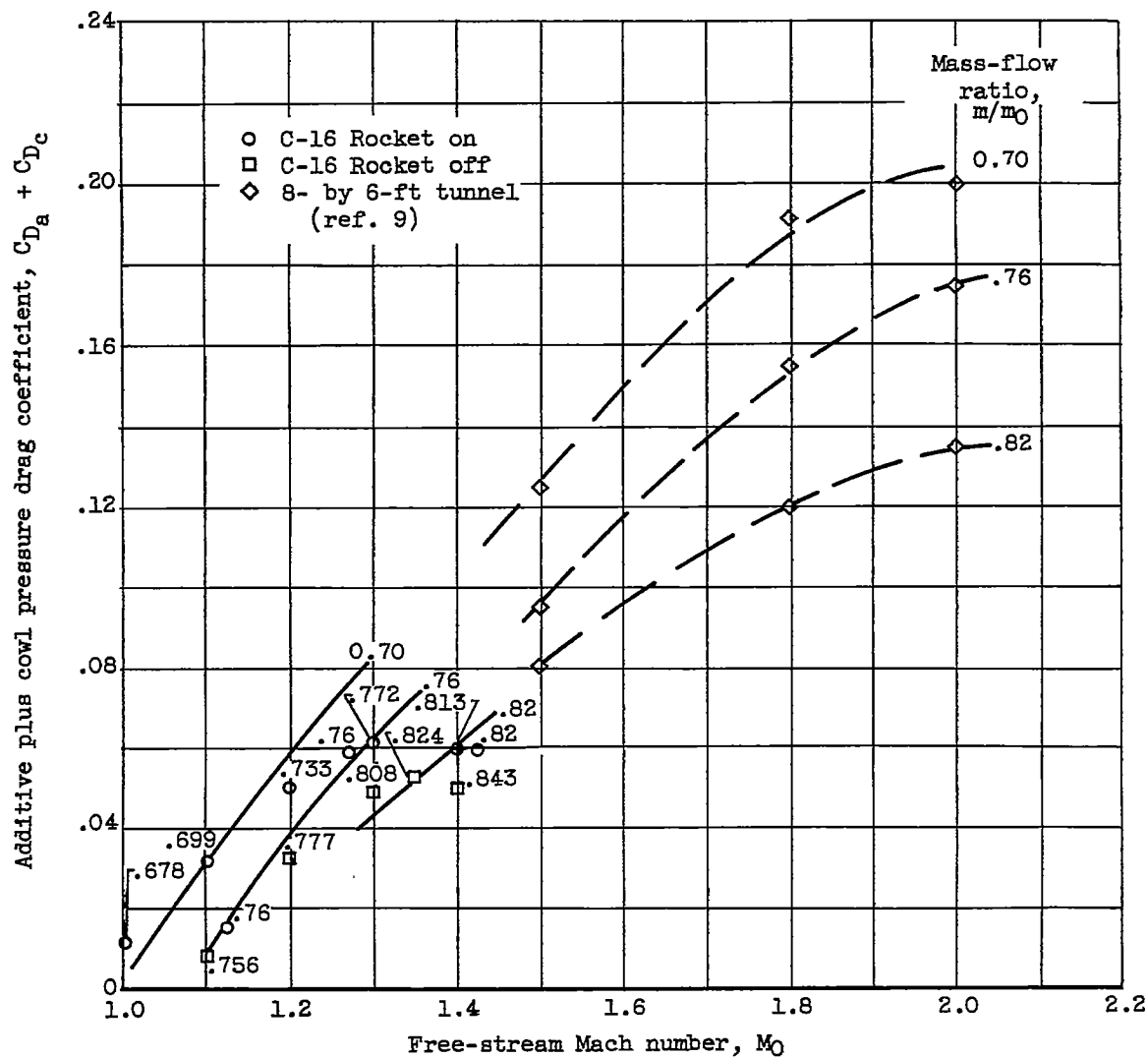
Figure 14. - Mass-flow-ratio correlation of component drag coefficients.
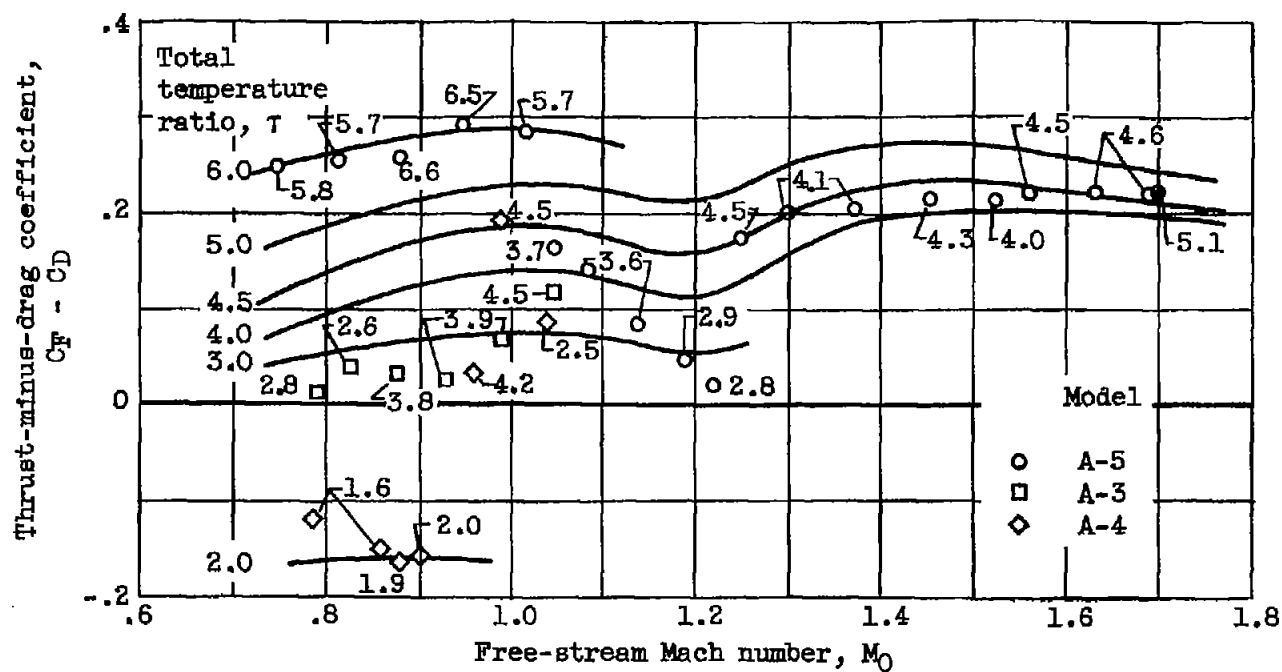
(a) Model A.

Figure 15. - Thrust-minus-drag coefficient as a function of Mach number for various τ.
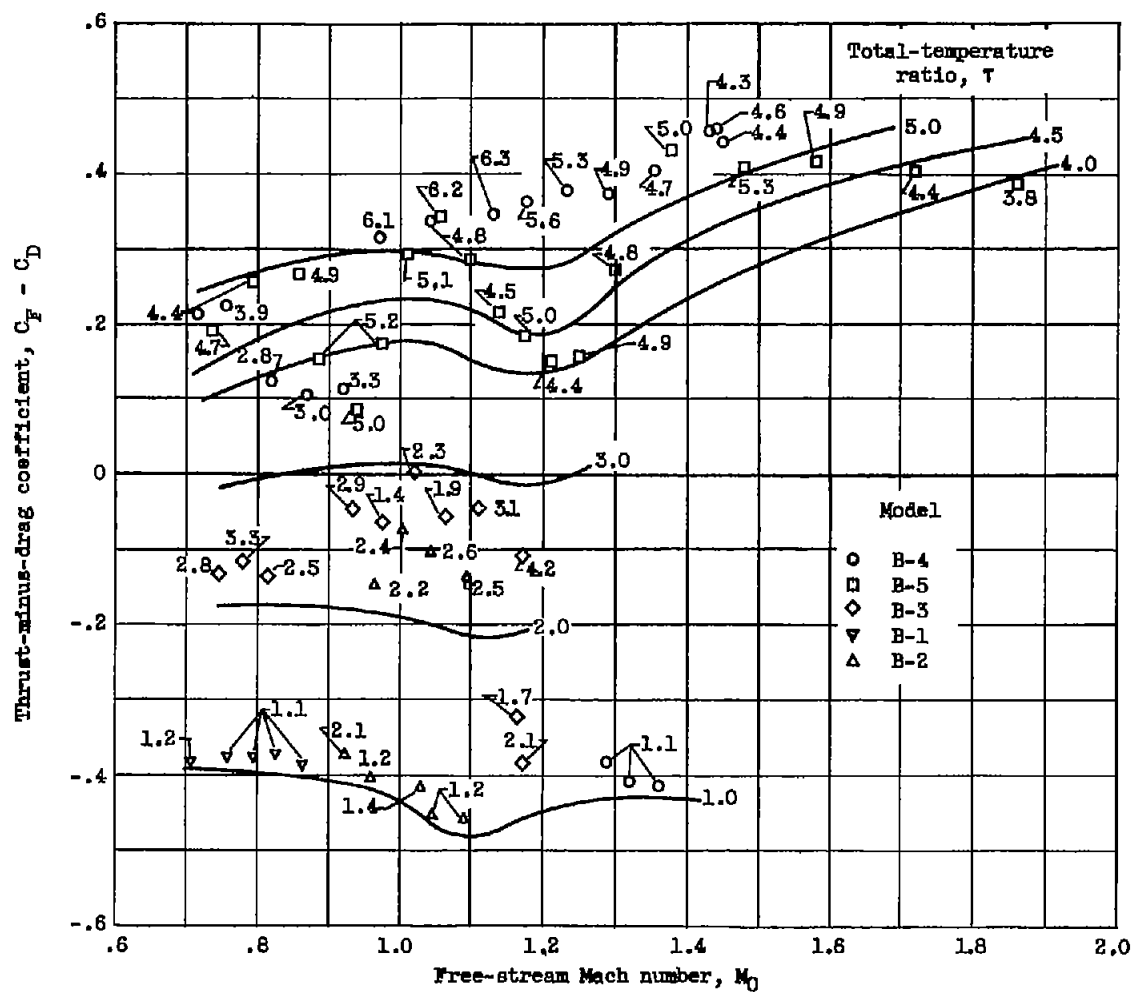
(b) Model B.

Figure 15. - Continued. Thrust-minus-drag coefficient as a function of Mach number for various τ.
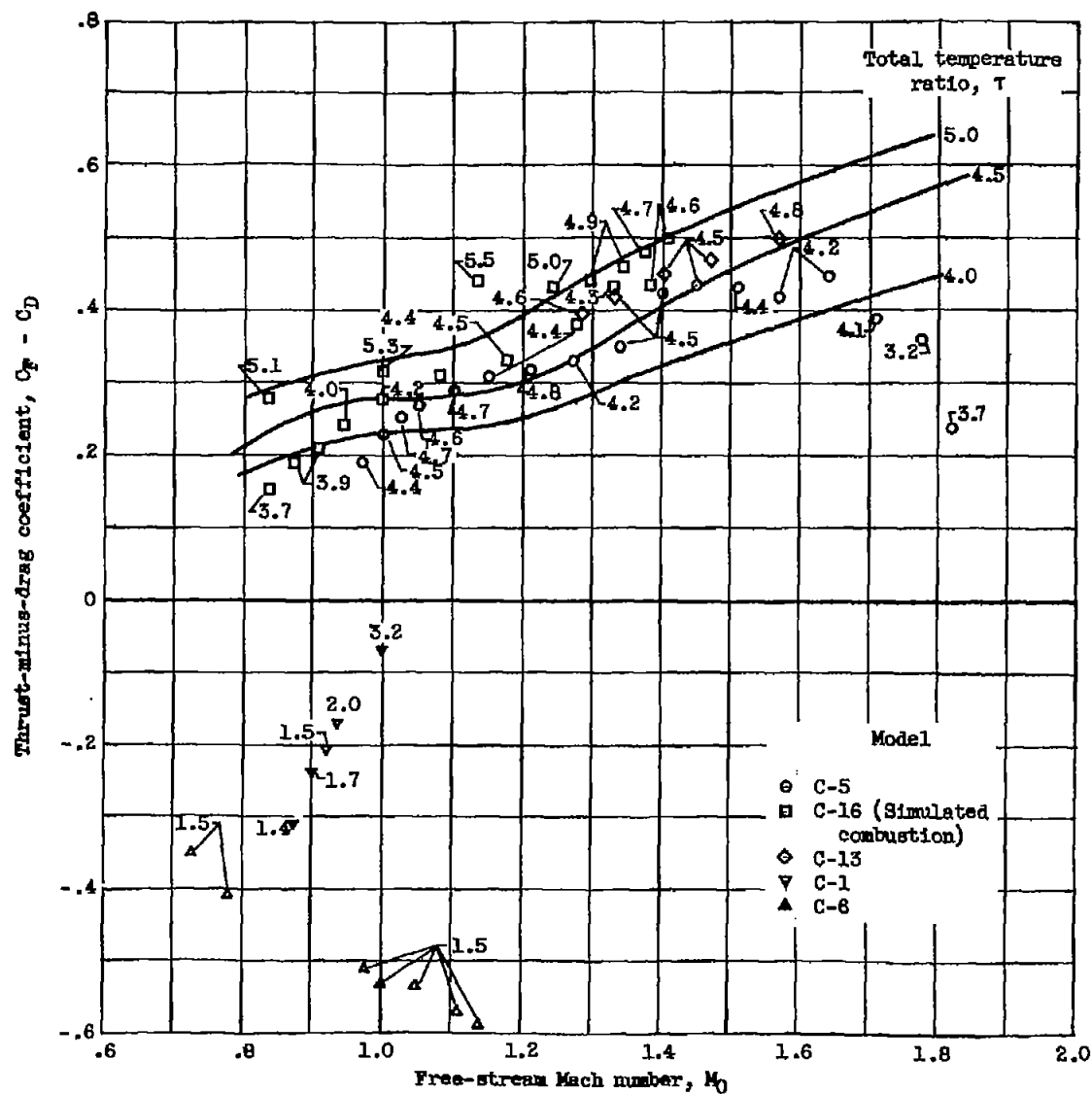
(c) Model C.

Figure 15. - Continued. Thrust-minus-drag coefficient as a function of Mach number for various τ.
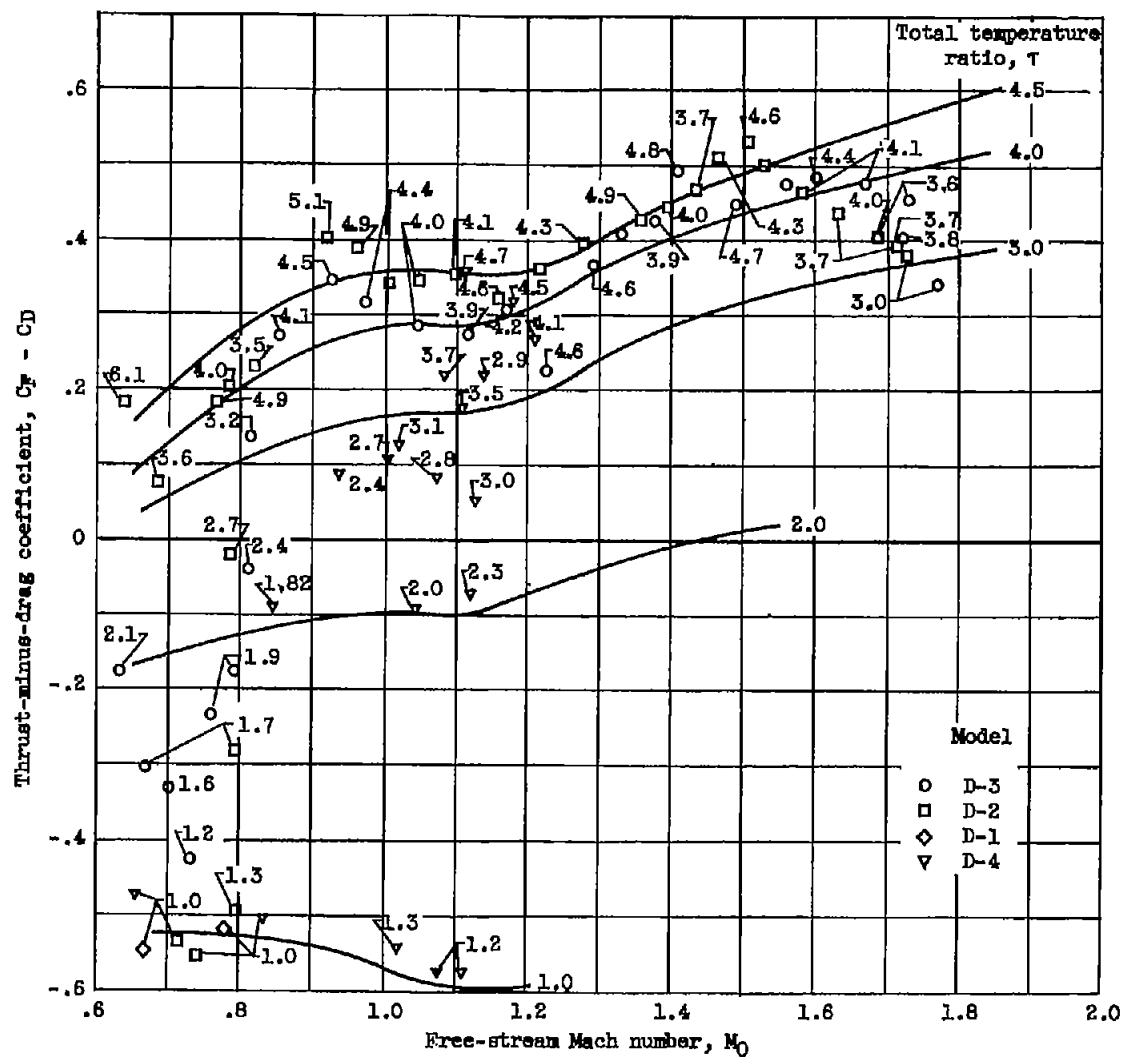
(d) Model D.

Figure 15. - Concluded. Thrust-minus-drag coefficient as a function of Mach number for various τ.
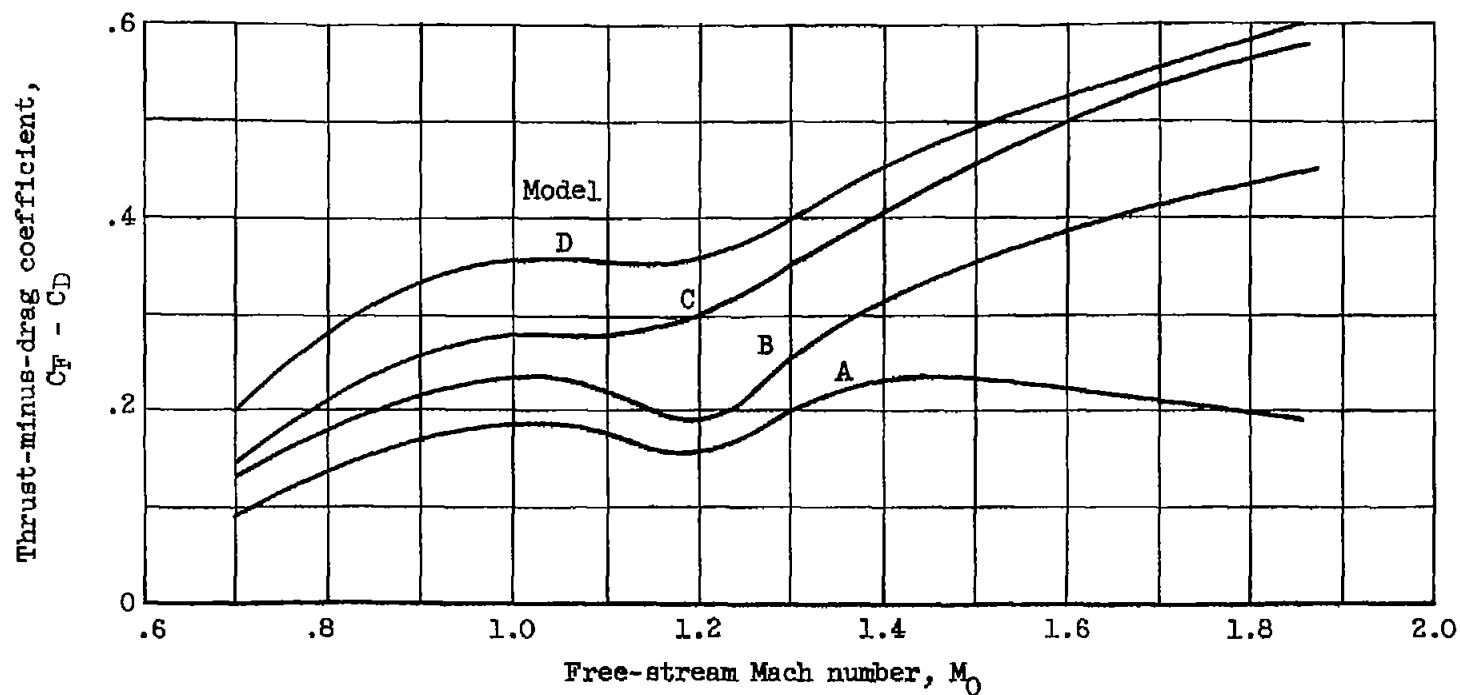
Figure 16. - Comparison of ram-jet thrust-minus-drag coefficients at total-temperature ratio of 4.5 for A, B, C, and D models.
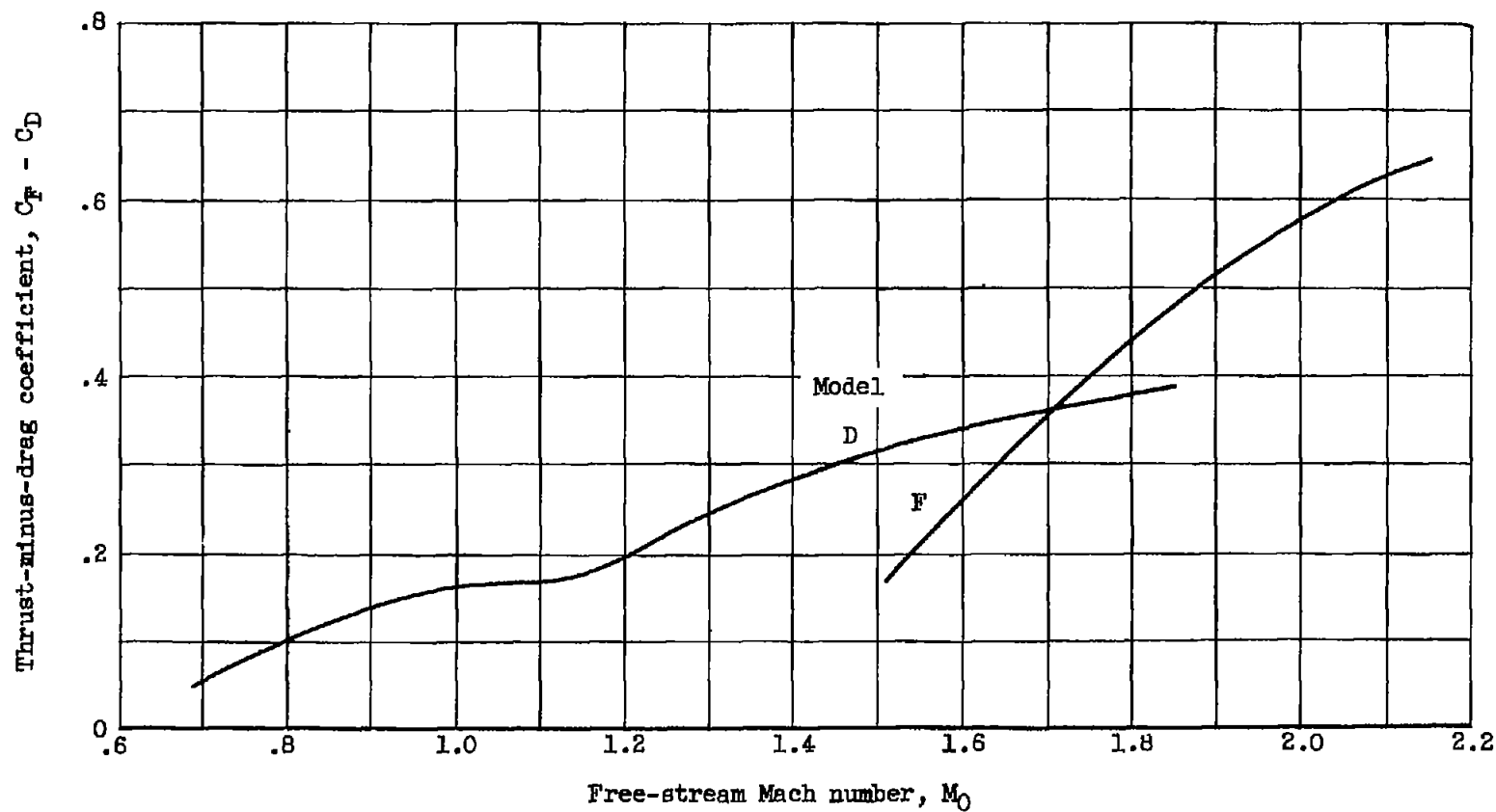
Figure 17. - Comparison of ram-jet thrust-minus-drag coefficients at total-temperature ratio of 3.0 for D and F models.
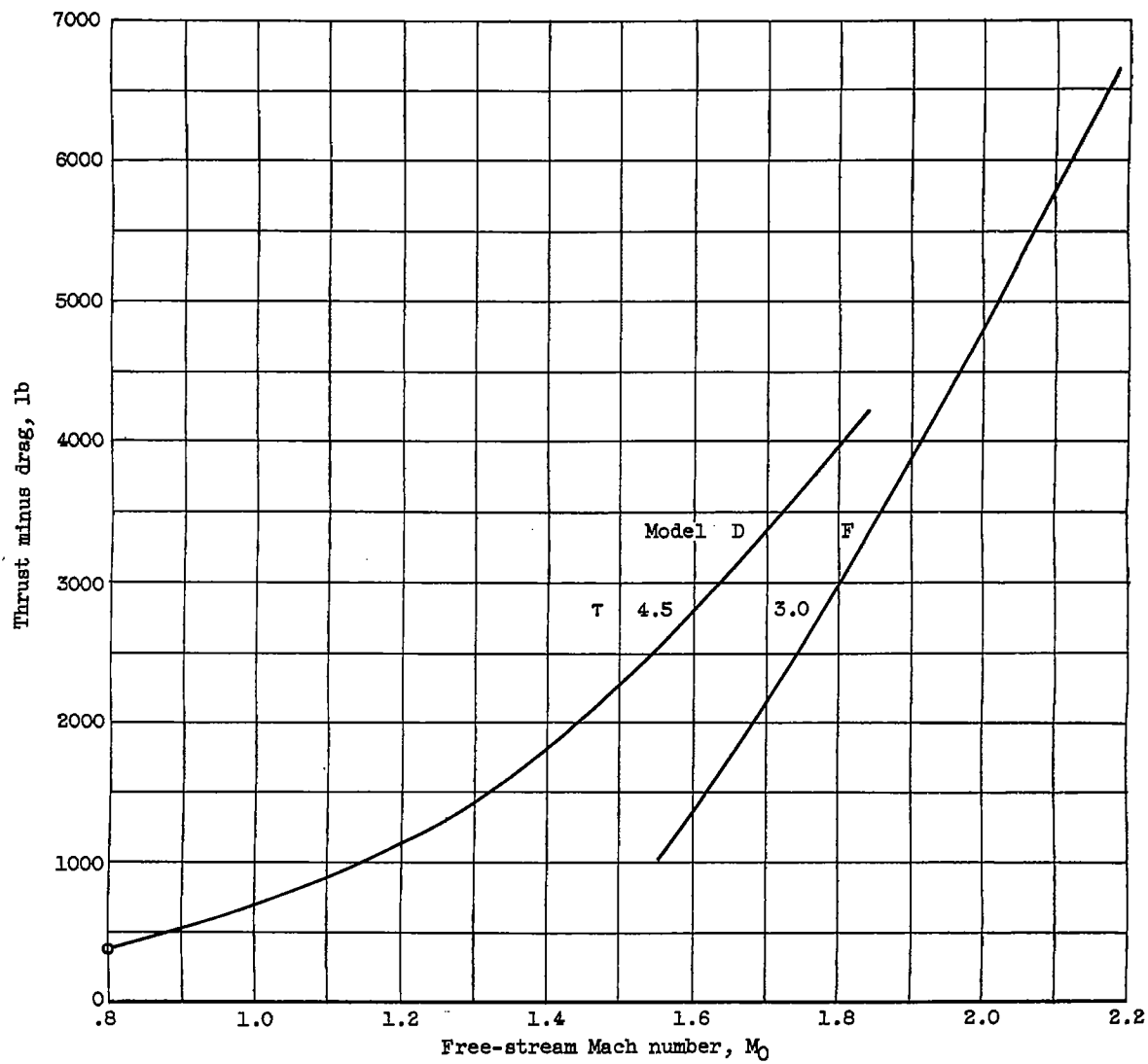
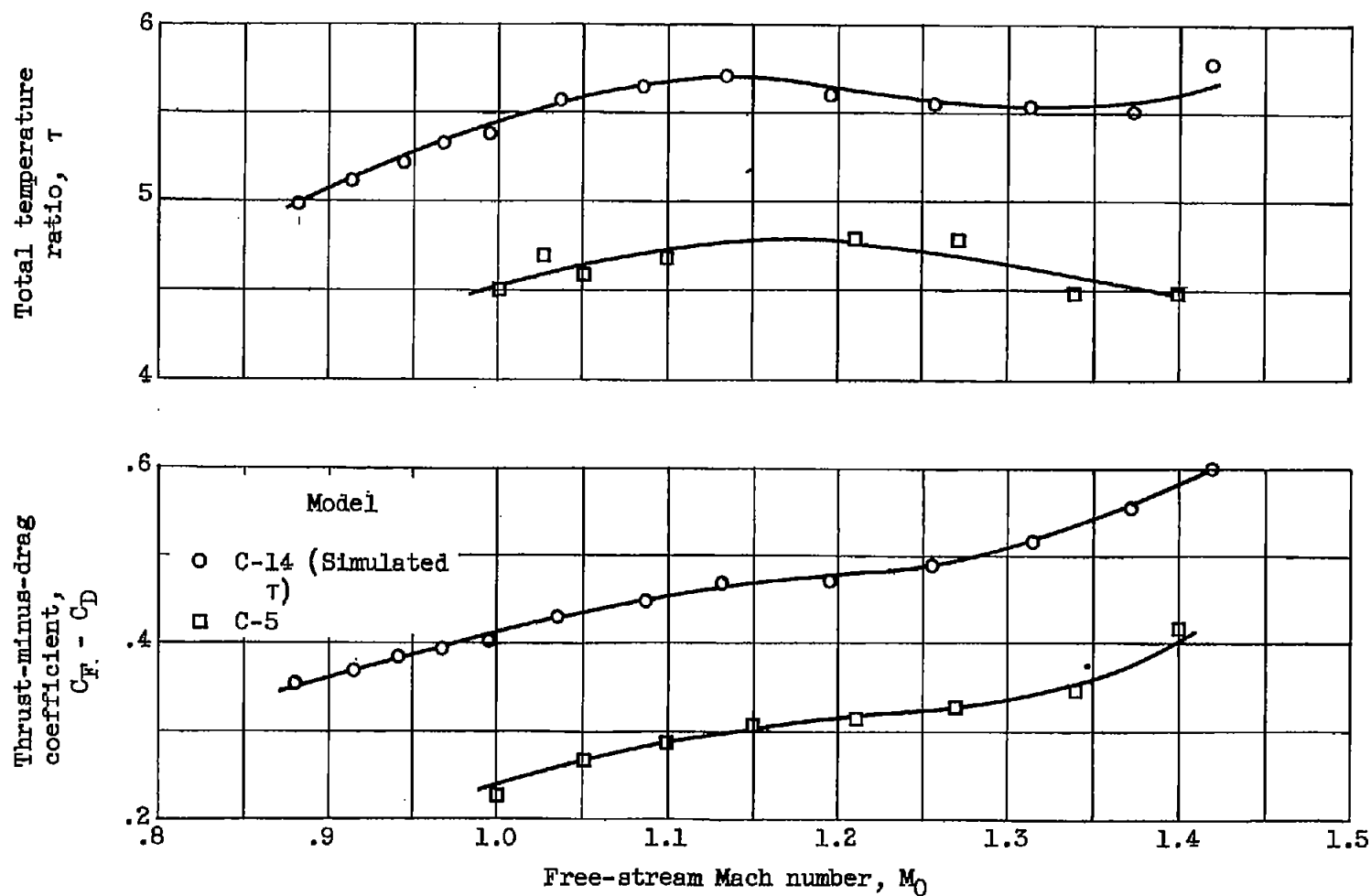Figure 18. - Sea-level propulsive thrust as a function of Mach number.

Figure 19. - Comparison of simulated and actual thrust-minus-drag coefficients as a function of Mach number.
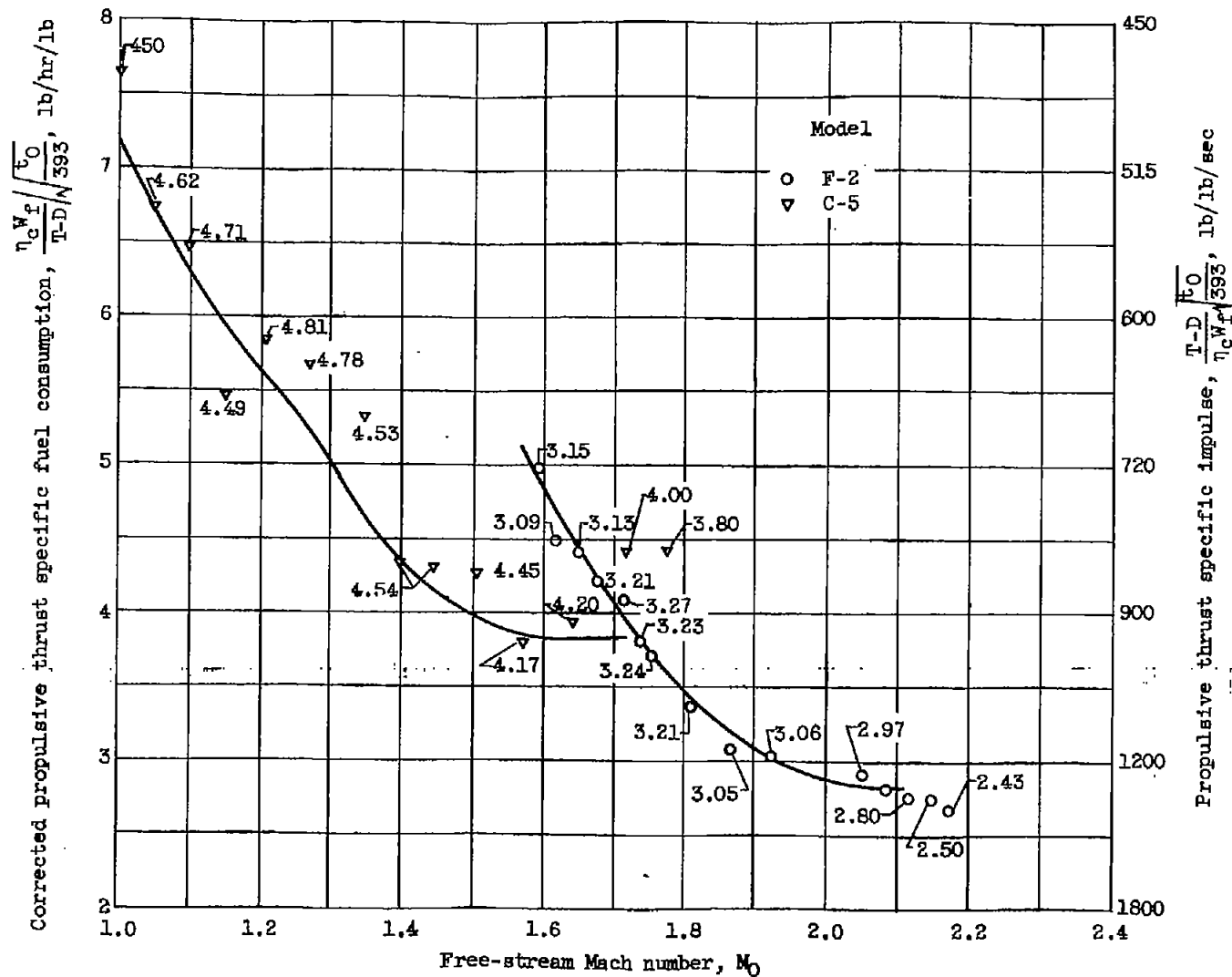
Figure 20. - Variation of corrected propulsive thrust specific fuel consumption and corrected propulsive thrust specific impulse with Mach number.
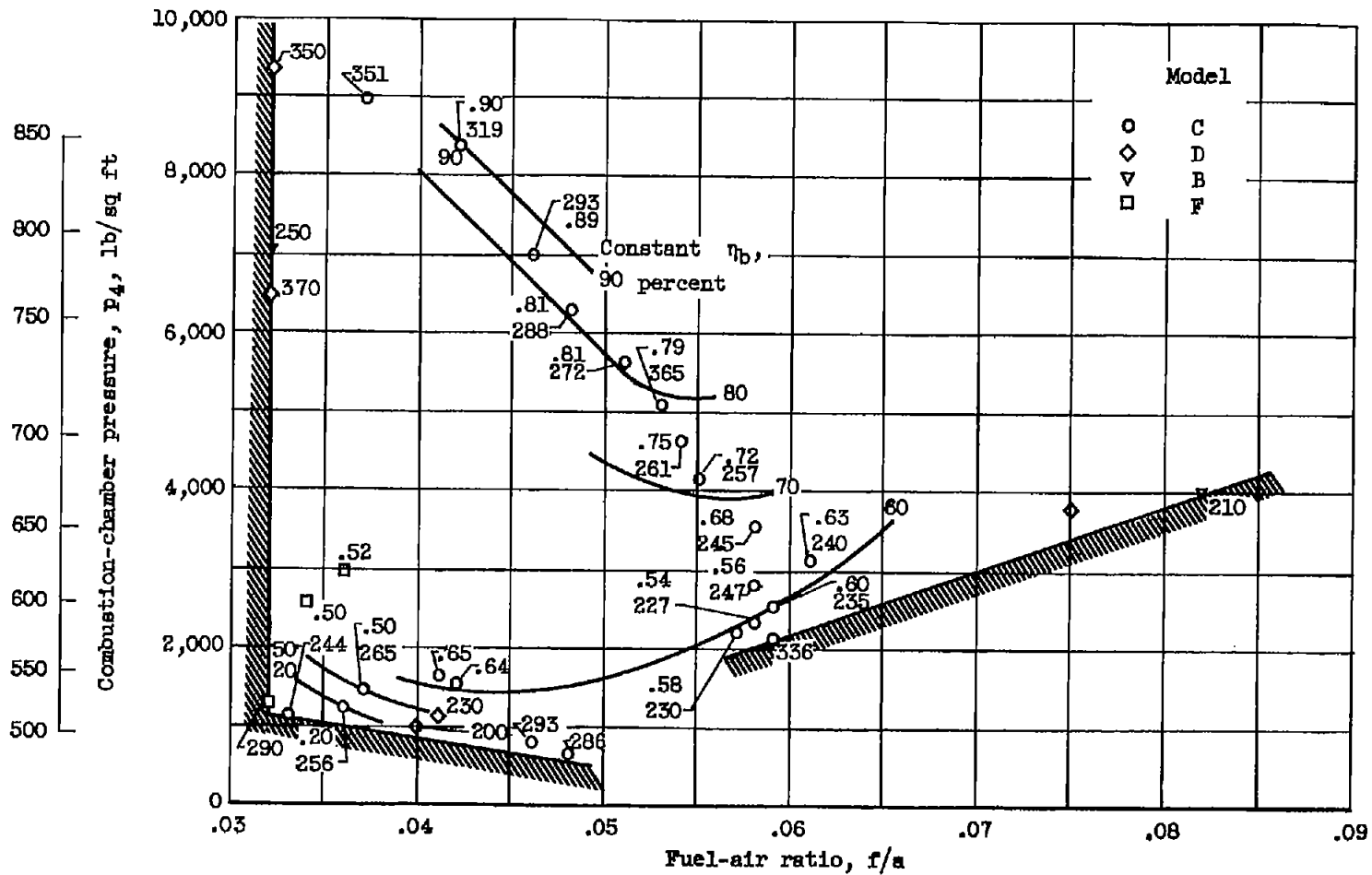
Figure 21. - Combustor performance. (Values for data points are combustion efficiency η_b, percent; combustion-chamber-inlet velocity V_4, ft/sec.)